JMEPEG (2010) 19:374–379
DOI: 10.1007/s11665-009-9490-y

1059-9495/$19.00

Extension of the Optical Absorption Range in Zn-Doped MgO Powders and Its Effect on Antibacterial Activity

Toshiaki Ohira, Mari Kawamura, Masayuki Fukuda, Kelly Alvarez, Burak Özkal, and Osamu Yamamoto

(Submitted September 23, 2008; in revised form March 13, 2009)

In order to produce powder samples of Zn-doped MgO, the precursors, MgO and ZnO, were mixed in a molar ratio higher than 1.86 and subsequently treated at 1200 °C for 5 h in air atmosphere. With increasing Zn content in MgO, the lattice constant increased linearly, and the optical absorption intensity increased in the wavelength ranging from 200 to 400 nm. Antibacterial activity of the obtained powder samples was examined by colony count method using *Escherichia coli* and *Staphylococcus aureus*. In the antibacterial tests, it was found that the antibacterial activity enhanced with increasing Zn content in MgO. Antibacterial action toward *S. aureus* was greater than that toward *E. coli*, irrespective of the Zn content in MgO. From these results, the enhancement of the antibacterial activity could be related with the optical absorption of Zn-doped MgO.

Keywords antibacterial activity, lattice constant, powders, solid solution, UV-vis, Zn-doped MgO

1. Introduction

Many inorganic antibacterial materials have been developed to prevent bio-infectious diseases (Ref 1-3). In almost all articles published so far, titanium dioxide (TiO_2) with anatase structure has been studied as an antibacterial material and attracted a great deal of attention, because TiO_2 when exposed to ultraviolet radiation below 360 nm generated holes (h^+) and excited electron (e^-) near its surface, i.e., photocatalysis (Ref 4-6). The production of active oxygen species such as super-oxide and hydroxyl radicals induced from the generated hole-electron pair was effective for the occurrence of antibacterial activity (Ref 7, 8).

On the other hand, magnesium oxide (MgO) also is one of the oxide ceramics that have great antibacterial activity without the presence of light (Ref 9-11). The antibacterial mechanism has been assumed to be due to the generation of super-oxide anions (O_2^-) on the surface of MgO, and the increase in pH value with the hydration of MgO (Ref 12, 13). By the way, MgO has high band gap energy, which is 7.8 eV (Ref 14). Generally, band gap changes can be achieved by doping with different elements using materials with high band gap, such as SiO_2 and AlN (Ref 15, 16). Ahn et al. (Ref 17) also reported that lower band gap energy could be achieved by doping ZnO in MgO structure. If Zn-doped MgO can show a band gap energy as low as TiO_2 (3.2 eV), i.e., a wide absorption range of light, the antibacterial activity of MgO is expected to be more enhanced with the presence of light than without it. However, it is not yet clear how the change in antibacterial activity of MgO with dopant could be influenced by the band gap energy. In other words, it is important to ensure the effect of optical absorption on antibacterial activity of MgO, in order to develop strong inorganic antibacterial materials.

According to the phase diagram of MgO-ZnO system (Ref 18), the solubility limit of ZnO in MgO is at the molar ratio (MgO/ZnO) of 1.86; that is, Zn-doped MgO can be formed above this molar ratio. This implies that the introduction of Zn^{2+} ions into the lattice MgO might reduce the band gap energy of MgO.

In the present work, the powder samples of Zn-doped MgO were obtained by heat-treating MgO and ZnO precursors mixed in a molar ratio (MgO/ZnO) higher than 1.86. After that, the optical absorption of the obtained powder samples was examined. Antibacterial activity against gram-positive and gram-negative bacteria was studied by using the obtained powder samples, i.e., Zn-doped MgO, with emphasis on the relation between optical absorption and antibacterial activity.

2. Experimental

2.1 Preparation of Materials

MgO (Ube Chemical Ind, Ltd. purity; 99.9%) and ZnO (Nacalai Tesque, Inc. purity; 99.9%) were used as starting materials. Several compositions based on $Mg_{1-x}Zn_xO$ (x ranges from 0.10 to 0.35) were prepared stoichiometrically by the conventional solid-state reaction. The precursors, MgO and ZnO, were mixed in an agate mortar at different molar ratios (MgO/ZnO) of 9.00-1.86 for 10 min. The mixtures were heated in electric furnace at 1200 °C for 5 h in an alumina boat in air

Toshiaki Ohira, Mari Kawamura, Kelly Alvarez, and **Osamu Yamamoto**, Center for Geo-Environmental Science, Faculty of Engineering and Resource Science, Akita University, 1-1 Tegata Gakuen-machi, Akita 010-8502, Japan; **Masayuki Fukuda**, Division of Dentistry and Oral Surgery, Akita University Hospital, 1-1-1 Hondo, Akita 010-8543, Japan; and **Burak Özkal**, Metallurgical and Materials Engineering Department, Faculty of Chemical and Metallurgical Engineering, Istanbul Technical University, 34469 Maslak Istanbul, Turkey. Contact e-mail: yamamoto@cges.akita-u.ac.jp.

atmosphere and then cooled to obtain three Zn-doped MgO, such as $Mg_{0.90}Zn_{0.10}O$, $Mg_{0.75}Zn_{0.25}O$ and $Mg_{0.65}Zn_{0.35}O$.

2.2 Powder Characterization

X-ray diffractometry (XRD; Rigaku, RAD-C System) equipped with a copper target ($\lambda_{K\alpha 1}$ = 0.15405 nm) was used to identify the formation phase of the obtained powder samples. The scanning rate was 1°/min from 2θ = 20-80° and the operation voltage and current of XRD were 40 kV and 20 mA, respectively. Lattice constant was calculated by using the (200) diffraction peaks of the powder samples detected on XRD. The lattice constant (a_0) of MgO and three Zn-doped MgO powders was calculated by Eq 1. In addition, the crystallite size was calculated by means of Scherrer equation.

$$a_0 = \left\{\left(h^2 + k^2 + l^2\right) \times d^2\right\}^{1/2} \quad \text{(Eq 1)}$$

where h, k, l are Miller indices and d is the interplane distance in nm.

Prior to the measurement of N_2 adsorption-desorption isotherms at −196 °C, the powder samples were pre-heated at 300 °C for 15 h in N_2 gas, in order to remove molecules adhering on the surface of powder samples. N_2 adsorption-desorption isotherms at −196 °C were measured (BET; BEL Japan, Inc. Belsorp-mini). Based on the BET analysis using experimental points measured at relative pressure (P/P_0) ranging from 0 to 0.50, the specific surface area of the powder samples was determined. For the determination of the optical energy band gap, the obtained powder samples were loaded into a quartz cell and the absorption spectra were measured by ultraviolet-visible spectrophotometer (UV-vis; JASCO, V-550) in the wavelength of 200-500 nm.

The measurement of pH when powder samples are added into water is important, because high pH value causes enhancement of the antibacterial activity (Ref 19-21). Powder samples were suspended in autoclaved water at the concentration of 0.63 g dm^{-3} to make powder slurries, and then a vial containing the powder slurries was kept in a water bath at 36 °C. The pH electrode (Mettler-Toledo Seven Easy) was inserted into the powder slurries. After keeping for 1 h, pH value of the slurries was measured.

2.3 Bacterial Suspension

Escherichia coli 745 (hereafter, *E. coli*) and *Staphylococcus aureus* 9779 (hereafter, *S. aureus*) were used in antibacterial tests. *E. coli* and *S. aureus* were cultured at 36 °C for 48 h in a LB medium. The LB medium is commonly used to culture gram-positive and gram-negative bacteria, it contains 0.5% yeast extract (Becton, Dickinson and Co.), 1% bactopeptone (Becton, Dickinson and Co.) and 1% sodium chloride (NaCl; Wako Pure Chemical Ind., Ltd, purity; 99.9%). The medium was rinsed four times with autoclaved water, and the bacterial culture was suspended in autoclaved water at a final concentration of 10^3 cfu dm^{-3}.

2.4 Viable Bacterial Count

The bacterial suspension was added into autoclaved water containing powder samples in the concentration from 0.08 to 1.25 g dm^{-3} and then kept at 36 °C for different times on a reciprocal shaker under fluorescent lamp. The light power was measured by a UV light meter (Fuso Co., Ltd.), which resulted to be 0.001 mW cm^{-2}. The bacterial suspension at a final concentration of 10^3 cfu dm^{-3} was spread on a nutrient agar (NA, Eiken Chemical, Co.) against *E. coli* and a pearl-core plate count agar (PPCA, Eiken Chemical, Co.) against *S. aureus*. The colonies formed on the agar were counted after the incubation at 36 °C for 48 h. The bacterial counts were carried out in duplicate on four different occasions and the average values of the four sampled data were plotted. In vitro antibacterial activity of the powder samples was assessed by the ratio (N/N_0) of the viable bacterial counts (N cfu dm^{-3}) at specified time divided by initial counts (control) of bacteria (N_0 cfu dm^{-3}).

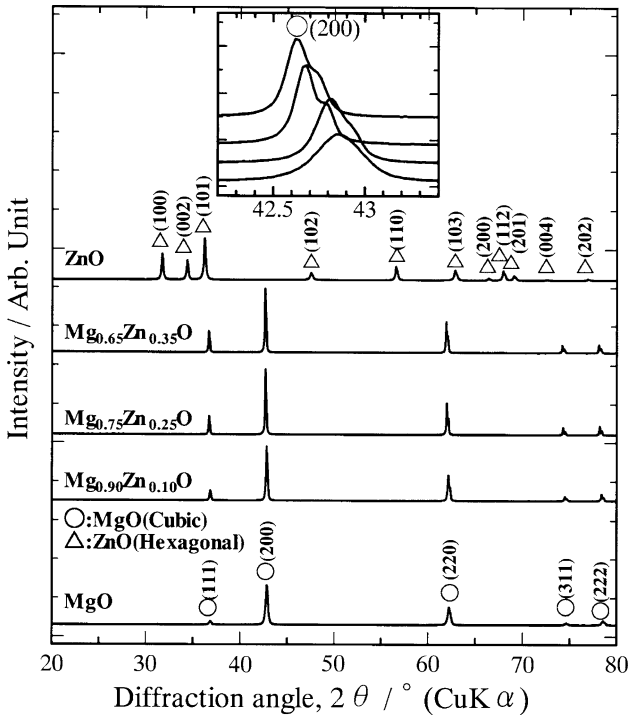

Fig. 1 XRD patterns of the powder samples obtained by heating at 1200 °C for 5 h in air

3. Results and Discussion

3.1 Powder Characterization

Figure 1 shows the XRD patterns of the Zn-doped MgO powders obtained at 1200 °C, together with the patterns of pure MgO and ZnO powders. Diffraction peaks corresponding to MgO with cubic type were detected in all powder samples, and there were no diffraction peaks corresponding to ZnO with hexagonal structure as a second phase. This indicates that Zn-doped MgO ($Mg_{1-x}Zn_xO$, x = 0.10-0.35) were successfully obtained with the preservation of the cubic structure. These peaks detected were recognized to shift to low-angle side with increasing Zn content in MgO, as can be clearly observed in the inset of Fig. 1. The presence of the amorphous halo that is a broad hump was not observed in the obtained XRD patterns. The change of the lattice constant, a_0, and the crystallite sizes of the obtained powder samples are shown in Fig. 2. The increase in lattice constant further confirms the formation of the Zn-doped MgO. According to Vegard's law, the value of the

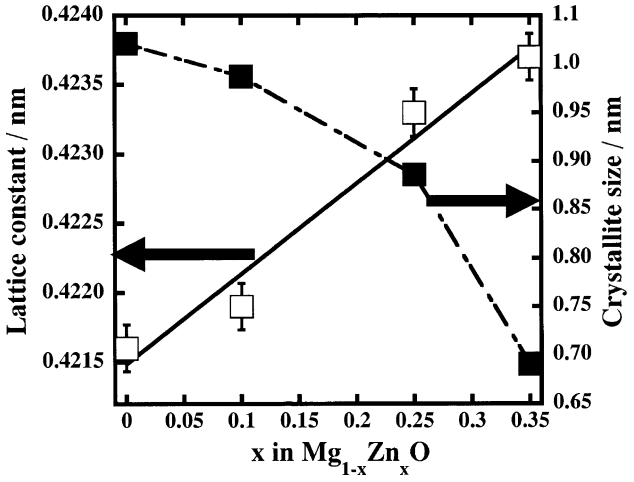

Fig. 2 Changes in lattice constant with Zn content in MgO

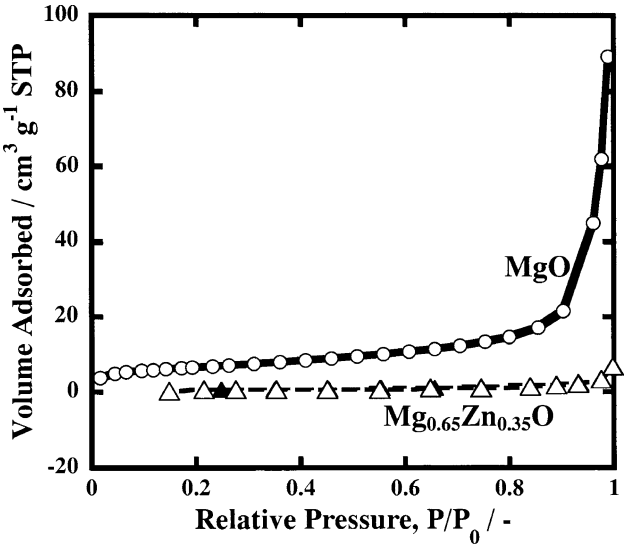

Fig. 3 N_2 adsorption-desorption isotherms at −196 °C on (a) MgO and (b) $Mg_{0.65}Zn_{0.35}O$

lattice constant increases linearly with increasing Zn content in MgO, which reached 0.4238 nm in $Mg_{0.65}Zn_{0.35}O$. The ionic radius of Zn^{2+} is slightly larger than that of Mg^{2+}, being 0.074 nm for Zn^{2+} ions and 0.071 nm for Mg^{2+} ions. The reason why the lattice constant of Zn-doped MgO moved toward larger values with increasing Zn content is presumed to be due to the substitution of Zn^{2+} ions to Mg^{2+} ions into the MgO lattice.

On antibacterial ceramics, one of the factors for the occurrence of the antibacterial activity has been assumed to be due to the generation of active oxygen species on its surface. In other words, the specific surface area of ceramics may affect the generating amount of active oxygen species. Therefore, measuring specific surface area of the obtained powder samples is important for evaluating antibacterial activity precisely. Figure 3 shows the obtained N_2 adsorption-desorption isotherms at −196 °C of pure MgO and $Mg_{0.65}Zn_{0.35}O$. It was found that the amount of N_2 adsorbed on MgO was much larger than that on $Mg_{0.65}Zn_{0.35}O$. By means of BET measurements, it was found that the specific surface area of Zn-doped MgO was smaller than that of MgO, showing the value of 24 m^2 g^{-1} for

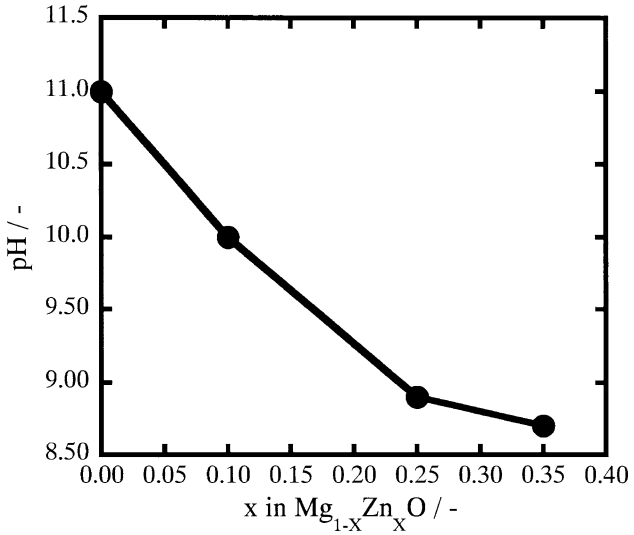

Fig. 4 Changes in pH value of Zn-doped MgO at powder concentration of 0.63 g dm^{-3}

pure MgO and 7.7 for $Mg_{0.90}Zn_{0.10}O$, 1.2 for $Mg_{0.75}Zn_{0.25}O$, and 2.3 for $Mg_{0.65}Zn_{0.35}O$. Since the specific surface area of the fabricated Zn-doped MgO powders was similar and the powders exhibited the same cubic structure, the effect of Zn content on the antibacterial activity can be determined.

Sawai et al. (Ref 22, 23) have reported that alkaline solution, such as NaOH aqueous solution, exhibited great bactericidal action with the enhancement of pH value. An aqueous solution containing MgO powder is known to show alkalinity due to the formation of $Mg(OH)_2$ with water. In addition, this fact along with the generation of active oxygen species is considered as one of the primary mechanisms of bactericidal action in MgO (Ref 24).

Measurement of the pH value in an aqueous solution containing powder samples was done to associate pH effect with the antibacterial activity. The results of the pH values with increasing Zn content in MgO are shown in Fig. 4. The pH value decreased with increasing Zn content in Zn-doped MgO.

3.2 Absorption Spectra of Powder Samples

The normalized absorption spectra of pure MgO and the fabricated Zn-doped MgO powders are shown in Fig. 5. The absorption spectra of Zn-doped MgO showed high UV intensity, in comparison with pure MgO. As shown in Fig. 5, the optical absorption was enhanced by increasing Zn content in MgO. In the wavelength ranging from 200 to 500 nm, any absorption peaks were observed for pure MgO. However, the absorption wavelength was extended to around 400 nm in Zn-doped MgO. With increasing Zn content in MgO, the absorption intensity became high. This result indicates that Zn-doped MgO absorbed light in the wavelength below 400 nm with high efficiency with increasing Zn content in MgO. Two absorption edges could be observed in all the fabricated Zn-doped MgO powders.

The optical band gap of the fabricated Zn-doped MgO was calculated using Tauc Model (Eq 2).

$$\alpha h\upsilon = A\left(h\upsilon - E_g\right)^r \quad \text{(Eq 2)}$$

where α is absorption of the fabricated Zn-doped MgO, $h\upsilon$ is the photon energy, E_g is the band gap energy, A is a constant

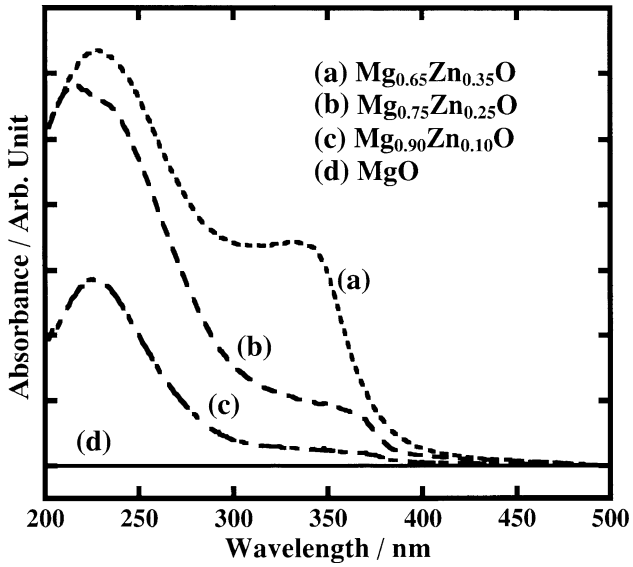

Fig. 5 UV-vis diffuse reflectance spectra of the pure MgO and Zn-doped MgO powders

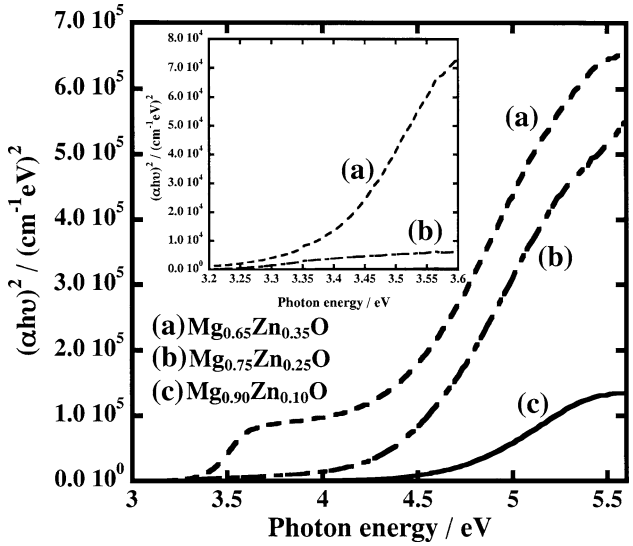

Fig. 6 $(\alpha h\upsilon)^2$ vs. $h\upsilon$ plots of the fabricated Zn-doped MgO

which does not depend on photon energy and r has four numeric values (1/2 for allowed direct, 2 for allowed indirect, 3 for forbidden direct and 3/2 for forbidden indirect optical transition).

In the estimation of the band gap, MgO is supposed to have direct band (Ref 25, 26). Zn-doped MgO has identical crystal structure with MgO. After we have plotted the $(\alpha h\upsilon)^2$ versus $h\upsilon$ for the fabricated Zn-doped MgO powders, the band gap was calculated by extrapolating the straight part of the plot to $(\alpha h\upsilon)^2 = 0$. From Fig. 6 it was observed that direct optical band gap was estimated as follows: 4.6 eV for $Mg_{0.90}Zn_{0.10}O$, 4.4 eV and 3.2 eV for $Mg_{0.75}Zn_{0.25}O$, and 4.2 and 3.4 eV for $Mg_{0.65}Zn_{0.35}O$, as summarized in Table 1. The change behavior of the band gap energy is presumed to be due to the charge-transfer transition between donor and acceptor ionization levels and the band continuum, which is reported in many literatures (Ref 27-29).

Table 1 Specific surface area and band gap energy on powder samples used in this work

Powder samples	Specific surface area, $m^2\ g^{-1}$	Band gap energy, eV
MgO	24	7.8 (Ref 14)
$Mg_{0.90}Zn_{0.10}O$	7.7	4.6
$Mg_{0.75}Zn_{0.25}O$	1.2	4.4, 3.2
$Mg_{0.65}Zn_{0.35}O$	2.3	4.2, 3.4

3.3 In Vitro Antibacterial Activity

Changes in antibacterial activity with increasing Zn content in MgO were evaluated by using powder samples at a powder concentration of 0.63 g dm^{-3}. Figure 7(a) and (b) shows the changes in survival ratio of *S. aureus* and *E. coli*, respectively. In the case of *S. aureus* (see Fig. 7a), the decline of the survival ratio on pure MgO was recognized to be slightly greater than that on $Mg_{0.90}Zn_{0.10}O$. With increasing Zn content in MgO, the survival ratio decreased steeply; that is, it can take the judgment that antibacterial action toward *S. aureus* enhanced with increasing Zn content in MgO. Thus, $Mg_{0.65}Zn_{0.35}O$ exhibited the greatest antibacterial activity among all the powder samples.

As described earlier, the specific surface area is an important powder characteristic affecting the antibacterial activity of the ceramics. The reason why pure MgO exhibited a stronger antibacterial activity in comparison with $Mg_{0.90}Zn_{0.10}O$ was presumed to be due to the highest specific surface area among all the obtained powder samples. However, the highest antibacterial activity was recognized for $Mg_{0.65}Zn_{0.35}O$, and the specific surface area was 2.3. In contrast, the specific surface area of MgO was much higher value (24 $m^2\ g^{-1}$) and the antibacterial activity of MgO was lower than that of $Mg_{0.65}Zn_{0.35}O$. This phenomenon suggests that specific surface area is not the effective characteristic in the antibacterial action, shown by the fabricated Zn-doped MgO powders.

The following three factors are known to affect the antibacterial activity of ceramics: (1) the cations eluted from ceramics, (2) the increase of pH values to alkaline values, (3) active oxygen species generated from ceramics (Ref 30). However, it was reported by Li et al. (Ref 31) that factor (1) had no effect on the activity of MgO. The changes of pH values shown in Fig. 4 indicated that the antibacterial activity did not enhance by the factor (2) but increased with the Zn content in MgO.

The occurrence of antibacterial activity on pure MgO has been reported to be due to active oxygen, O_2^-, generated from its surface, and any optical absorption peaks were recognized in the wavelength ranging from 200 to 500 nm. However, the fabricated Zn-doped MgO powders absorbed the light in the wavelength below 400 nm, which was similar to the band gap of TiO_2 (Ref 32), suggesting that Zn-doped MgO possessed the ability to function as a photo-catalyst like TiO_2. In the case of TiO_2, active oxygen species, such as O_2^-, H_2O_2, and $^{\bullet}OH$ are generated after exposition to ultraviolet radiation (Ref 33-36). The antibacterial activity is caused by attacking the cell wall of bacteria with the generated active oxygen species (Ref 37). Therefore, it is anticipated that the antibacterial activity of Zn-doped MgO occurred by the generation of active oxygen species from its surface. The absorption intensity increased with increasing Zn content in MgO, expecting the generation of large amount of active oxygen species. The reason why the

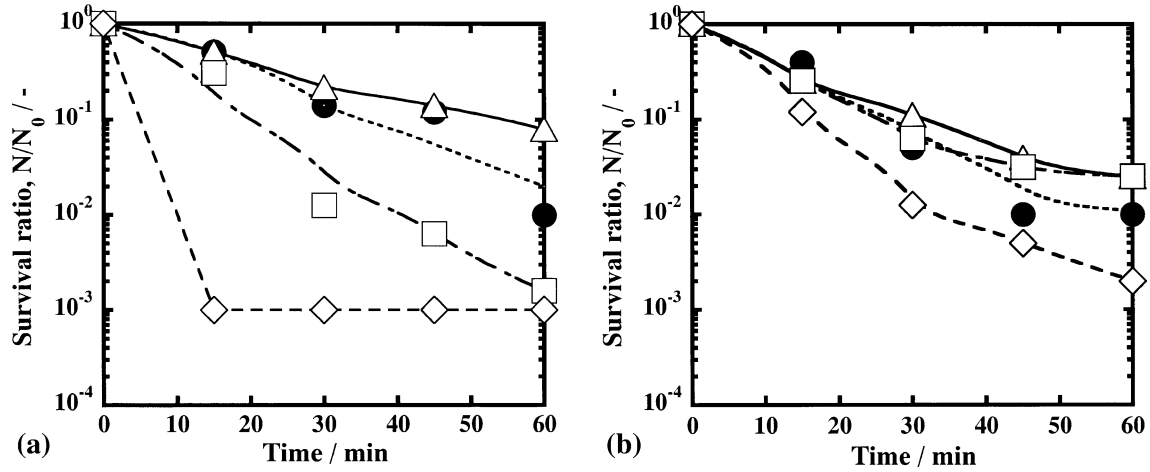

Fig. 7 Survival ratio of (a) *S. aureus* and (b) *E. coli* on Zn-doped MgO powders at powder concentration of 0.63 g dm^{-3}. (●) MgO, (△) $Mg_{0.90}Zn_{0.10}O$, (□) $Mg_{0.75}Zn_{0.25}O$, (◇) $Mg_{0.65}Zn_{0.35}O$

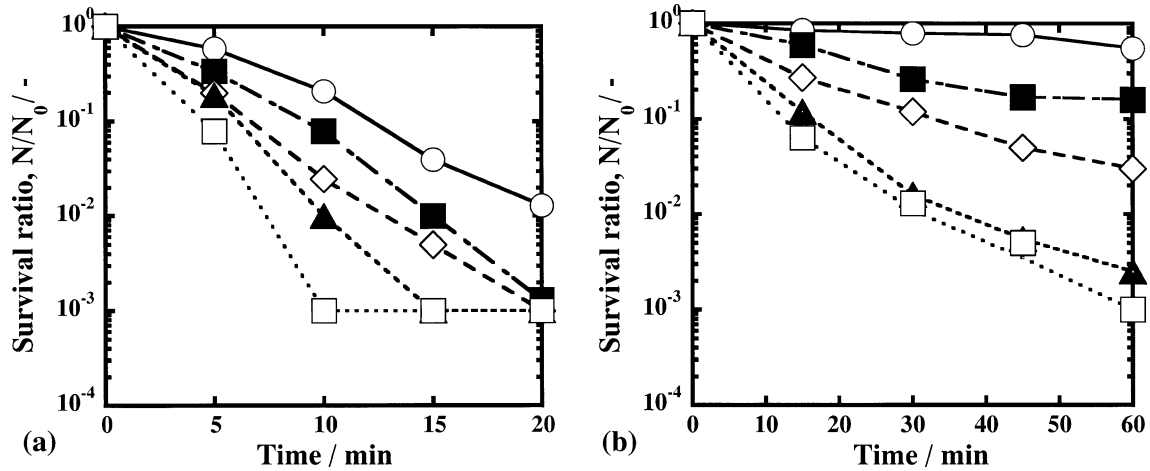

Fig. 8 Survival ratio of (a) *S. aureus* and (b) *E. coli* on $Mg_{0.65}Zn_{0.35}O$ with different powder concentrations. (○) 0.08 g dm^{-3}, (■) 0.16 g dm^{-3}, (◇) 0.32 g dm^{-3}, (▲) 0.63 g dm^{-3}, (□) 1.25 g dm^{-3}

antibacterial activity enhanced with increasing Zn content in MgO is presumed to be due to the large optical absorption in the wavelength below 400 nm.

The decline behavior of the survival ratio of *E. coli* was a little different from that of *S. aureus*, as shown in Fig. 7(b). That is, the survival ratio of *E. coli* did not show large difference during Zn-doped MgO, although the survival ratio on $Mg_{0.65}Zn_{0.35}O$ declined more than in the other samples. In comparison during Zn-doped MgO having same Zn content, the survival ratio of *E. coli* is greater than that of *S. aureus*. This indicates that the antibacterial action toward *S. aureus* is greater than that toward *E. coli*.

The structure and the chemical compositions of the cell surface are quite different between *E. coli* and *S. aureus*. The cell surface of *E. coli* consists of the thin layers of lipid A, lipopolysaccharide, and peptidoglycan. However, *S. aureus* consists of only a peptidoglycan layer. Membrane function, activity of enzymes associated with membrane, and maintenance of cell integrity depend on the surface of the cell surface. *E. coli* showed a comparatively great resistance for antibiotics, and *S. aureus* was weak in chemical stress (Ref 38). In other words, the sensitivity of *S. aureus* to antibiotics is higher than *E. coli*. The reason why Zn-doped MgO showed greater antibacterial activity against *S. aureus* than that against *E. coli* is presumed to be due to the high sensitivity to active oxygen species.

The survival ratio on the powder concentration of Zn-doped MgO was examined by using $Mg_{0.65}Zn_{0.35}O$ that showed greatest antibacterial activity in all samples. The survival ratio of *S. aureus* and *E. coli* is shown in Fig. 8(a) and (b), respectively. The survival ratio was found to decrease steeply with increasing powder concentration, irrespective of the kind of bacteria. This result is assumed to be due to the quantitative increase of active oxygen species occurred by increasing powder concentration.

4. Conclusions

Zn-doped MgO powders ($Mg_{1-x}Zn_xO$) were prepared in molar ratio (MgO/ZnO) higher than 1.86 without the formation of a second phase of ZnO and the antibacterial activity was examined by using *E. coli* and *S. aureus*. $Mg_{0.65}Zn_{0.35}O$

exhibited great antibacterial activity against both *E. coli* and *S. aureus*, resulting to be more effective than MgO. With increasing Zn content in Zn-doped MgO powders, the optical absorption intensity increased in the wavelength ranging from 200 to 400 nm. The antibacterial activity enhanced with increasing Zn content in Zn-doped MgO. From these results, a good relationship between antibacterial activity and optical absorption was found in Zn-doped MgO powders.

References

1. J. Sawai, H. Igarashi, A. Hashimoto, T. Kokugan, and M. Shimizu, Evaluation of Growth Inhibitory Effect of Ceramics Powder Slurry on Bacteria by Conductance Method, *J. Chem. Eng. Jpn.*, 1995, **28**, p 288–293
2. O. Yamamoto, T. Fukuda, M. Kimata, J. Sawai, and T. Sasamoto, Antibacterial Characteristics of MgO-Mounted Spherical Carbon by Carbonization of Ion-Exchanged Resin, *J. Ceram. Soc. Jpn.*, 2001, **109**, p 363–365
3. O. Seven, B. Dindar, S. Aydemir, D. Metin, M.A. Ozinel, and S. Ichii, Solar Photocatalytic Disinfection of a Group of Bacteria and Fungi Aqueous Suspensions with TiO_2, ZnO and Sahara Desert Dust, *J. Photochem. Photobiol. A: Chem.*, 2004, **165**, p 103–107
4. C. Wang, A. Heller, and H. Gerischer, Palladium Catalysis of O_2 Reduction by Electrons Accumulated on TiO_2 Particle During Photo-assisted Oxidation of Organic Compounds, *J. Am. Chem. Soc.*, 1992, **114**, p 5230–5234
5. B. Tryba, A.W. Morawski, T. Tsumura, M. Toyoda, and M. Inagaki, Hybridization of Adsorptivity with Photocatalytic Activity—Carbon-Coated Anatase, *J. Photochem. Photobiol. A: Chem.*, 2004, **167**, p 127–135
6. Y.-B. Xie and X.-Z. Li, Degradation of Bisphenol A in Aqueous Solution by H_2O_2-Assisted Photoelectrocatalytic Oxidation, *J. Hazard. Mater. B*, 2006, **138**, p 526–533
7. L.K. Adams, D.Y. Lyon, and P.J.J. Alvarez, Comparative Eco-Toxicity of Nanoscale TiO_2, SiO_2 and ZnO Water Suspensions, *Water Res.*, 2006, **40**, p 3527–3532
8. L. Armelao, D. Barreca, G. Bottaro, A. Gasparotto, C. Maccato, C. Maragno, E. Tondello, U.L. Stangar, M. Bergant, and D. Mahne, Photocatalytic and Antibacterial Activity of TiO_2 and Au/TiO_2 Nanosystems, *Nanotechnology*, 2007, **18**, p 1–7
9. J. Sawai, H. Igarashi, A. Hashimoto, T. Kokugan, and M. Shimizu, Effect of Ceramic Powder Slurry on Spores of *Bacillus Subtilis*, *J. Chem. Eng. Jpn.*, 1995, **28**, p 556–561
10. J. Sawai, H. Igarashi, A. Hashimoto, T. Kokugan, and M. Shimizu, Effect of Particle Size and Heating Temperature of Ceramic Powders on Antibacterial Activity of Their Slurries, *J. Chem. Eng. Jpn.*, 1996, **29**, p 251–256
11. J. Sawai, H. Kojima, H. Igarashi, A. Hashimoto, S. Shoji, A. Takehara, T. Sawaki, T. Kokugan, and M. Shimizu, *Escherichia coli* Damage by Ceramic Powder Slurries, *J. Chem. Eng. Jpn.*, 1997, **30**, p 1034–1039
12. J. Sawai, Quantitative Evaluation of Antibacterial Activities of Metallic Oxide Powders (ZnO, MgO and CaO) by Conductimetric Assay, *J. Microbiol. Methods*, 2003, **54**, p 177–182
13. J. Sawai, H. Kojima, N. Ishizu, M. Itoh, H. Igarashi, T. Sawaki, and M. Shimizu, Bactericidal Action of Magnesium Oxide Powder, *J. Inorg. Biochem.*, 1997, **71**, p 443
14. G. Cappellini, F. Finocchi, S. Bouette-Russo, and C. Noguera, Ground-State Properties and Excitation Energies of Cubic SrO and MgO, *Comput. Mater. Sci.*, 2001, **20**, p 401–406
15. A.Y. Polyakov, N.B. Smirnov, and A.V. Govorkov, Properties of Highly Cr-Doped AlN, *Appl. Phys. Lett.*, 2004, **85**, p 4067–4069
16. N. Chiodini, A. Paleari, G. Spinolo, and P. Crespi, Photorefractivity in SiO_2:SnO_2 Glass-Ceramics by Visible Light, *J. Non-Cryst. Solids*, 2003, **322**, p 266–271
17. S.G. Ahn, S.H. Yoon, and Y.S. Kim, Secondary Electron Emission Characteristics of MgO-ZnO Alloy Thin Film Layer for AC PDP, *Thin Solid Films*, 2009, **517**, p 4027–4030
18. E.R. Segnit and A.E. Holland, The System of MgO-ZnO-SiO_2, *J. Am. Ceram. Soc.*, 1965, **48**, p 409–412
19. P. Small, D. Blankenhorn, D. Welty, E. Zinser, and J.L. Slonczewski, Acid and Base Resistance in *Escherichia coli* and *Shigella flexneri*: role of rpoS and Growth pH, *J. Bacteriol.*, 1994, **176**, p 1729–1737
20. C.W. Chang, W.L. Chang, and S.T. Chang, Influence of pH on Bioactivity of Cinnamon Oil Against *Legionella pneumophila* and Its Disinfection Efficacy in Hot Springs, *Water Res.*, 2008, **42**, p 5022–5030
21. C. Estrela, F.C. Pimenta, I.Y. Ito, and L.L. Bammann, In Vitro Determination of Direct Antimicrobial Effect of Calcium Hydroxide, *J. Endodont.*, 1998, **24**, p 15–17
22. J. Sawai, H. Shiga, and H. Kojima, Kinetic Analysis of Death of Bacteria in CaO Powder Slurry, *Int. Biodeter. Biodegr.*, 2001, **47**, p 23–26
23. J. Sawai, K. Himizu, and O. Yamamoto, Kinetics of Bacterial Death by Heated Dolomite Powder Slurry, *Soil Biol. Biochem.*, 2005, **37**, p 1484–1489
24. J. Sawai, H. Kojima, H. Igarashi, A. Hashimoto, S. Shoji, T. Sawaki, A. Hakoda, E. Kawada, T. Kokugan, and M. Shimizu, Antibacterial Characteristics of Magnesium Oxide Powder, *J. Microbiol. Biotechnol.*, 2000, **16**, p 187–194
25. S.H. Tamboli, R.B. Patil, S.V. Kamat, Vijaya Puri, and R.K. Puri, Modification of Optical Properties of MgO Thin Films by Vapor Chopping, *J. Alloys Compd.*, 2009, **477**, p 855–859
26. S. Jalili and R. Majidi, The Effect of Impurities on Electronic Properties of MgO, *Physica B*, 2008, **403**, p 3522–3526
27. A. Ohtomo, M. Kawasaki, T. Koida, K. Masabuchi, and H. Koinuma, $Mg_XZn_{1-X}O$ as a II-VI Widegap Semiconductor Alloy, *Appl. Phys. Lett.*, 1998, **72**, p 2466–2468
28. T. Fukumura, Z. Jin, A. Ohtomo, H. Koinuma, and M. Kawasaki, An Oxide-Diluted Magnetic Semiconductor: Mn-doped ZnO, *Appl. Phys. Lett.*, 1999, **75**, p 3366–3368
29. S. Gao, X. Zhang, Y. Huang, Y. Li, and Z. Du, Investigation on Electronic Structures and Nature of Charge-Transfer Transition of ZnO: Co with Variation of Co Content, *Chem. Phys. Lett.*, 2008, **459**, p 82–84
30. J. Sawai, E. Kawada, F. Kanou, H. Igarashi, A. Hashimoto, T. Kokugan, and M. Shimizu, Detection of Active Oxygen Generated from Ceramic Powders Having Antibacterial Activity, *J. Chem. Eng. Jpn.*, 1996, **29**, p 627–633
31. L. Li, J. Gao, and Y. Wang, Evaluation of Cyto-Toxicity and Corrosion Behavior of Alkali-Heat-Treated Magnesium in Simulated Body Fluid, *Surf. Coat. Technol.*, 2004, **185**, p 92–98
32. M.M. Hasan, A.S.M.A. Haseeb, R. Saidur, and H.H. Masjuki, Effects of Annealing Treatment on Optical Properties of Anatase TiO_2 Thin Films, *Int. J. Chem. Biomol. Eng.*, 2008, **1**, p 93–97
33. B.G. Kwon, Characterization of the Hydroperoxyl/Superoxide Anion Radical ($HO_2./O_2.^-$) Formed from the Photolysis of Immobilized TiO_2 in a Continuous Flow, *J. Photochem. Photobiol. A: Chem.*, 2008, **199**, p 112–118
34. P.A. Pekakis, N.P. Xekoukoulotakis, and D. Mantzavinos, Treatment of Textile Dyehouse Wastewater by TiO_2 Photocatalysis, *Water Res.*, 2006, **40**, p 1276–1286
35. I.K. Konstantinou and T.A. Albanis, TiO_2-Assisted Photocatalytic Degradation of Azo Dyes in Aqueous Solution: Kinetic and Mechanistic Investigations, *Appl. Catal. B: Environ.*, 2004, **49**, p 1–14
36. K. Ishibashi, Y. Nosaka, K. Hashimoto, and A. Fujishima, Time-Dependent Behavior of Active Oxygen Species Formed on Photoirradiated TiO_2 Films in Air, *J. Phys. Chem. B*, 1998, **102**, p 2117–2120
37. P.-C. Maness, S. Smolinski, D.M. Blake, Z. Huang, E.J. Wolfrum, and W.A. Jacoby, Bactericidal Activity of Photocatalytic TiO_2 Reaction: Toward Understanding of Its Killing Mechanism, *Appl. Environ. Microbiol.*, 1999, **65**, p 4094–4098
38. F. Brill, P. Goroncy-Bermes, and W. Sand, Influence of Growth Media on the Sensitivity of *Staphylococcus aureus* and *Pseudomonas aeruginosa* to Cationic Biocides, *Int. J. Hyg. Environ. Health*, 2006, **209**, p 89–95